

Fluctuations of cytoskeleton-bound microbeads—the effect of bead–receptor binding dynamics

C Metzner, C Raupach, C T Mierke and B Fabry¹

Center for Medical Physics and Technology, University of Erlangen-Nuremberg, Erlangen, Germany

E-mail: bfabry@biomed.uni-erlangen.de

Received 13 October 2009, in final form 20 January 2010

Published 26 April 2010

Online at stacks.iop.org/JPhysCM/22/194105

Abstract

The cytoskeleton (CSK) of living cells is a crosslinked fiber network, subject to ongoing biochemical remodeling processes that can be visualized by tracking the spontaneous motion of CSK-bound microbeads. The bead motion is characterized by anomalous diffusion with a power-law time evolution of the mean square displacement (MSD), and can be described as a stochastic transport process with apparent diffusivity D and power-law exponent β : $\text{MSD} \sim D(t/t_0)^\beta$. Here we studied whether D and β change with the time that has passed after the initial bead–cell contact, and whether they are sensitive to bead coating (fibronectin, integrin antibodies, poly-L-lysine, albumin) and bead size (0.5–4.5 μm). The measurements are interpreted in the framework of a simple model that describes the bead as an overdamped particle coupled to the fluctuating CSK network by an elastic spring. The viscous damping coefficient characterizes the degree of bead internalization into the cell, and the spring constant characterizes the strength of the binding of the bead to the CSK. The model predicts distinctive signatures of the MSD that change with time as the bead couples more tightly to the CSK and becomes internalized. Experimental data show that the transition from the unbound to the tightly bound state occurs in an all-or-nothing manner. The time point of this transition shows considerable variability between individual cells (2–30 min) and depends on the bead size and bead coating. On average, this transition occurs later for smaller beads and beads coated with ligands that trigger the formation of adhesion complexes (fibronectin, integrin antibodies). Once the bead is linked to the CSK, however, the ligand type and bead size have little effect on the MSD. On longer timescales of several hours after bead addition, smaller beads are internalized into the cell more readily, leading to characteristic changes in the MSD that are consistent with increased viscous damping by the cytoplasm and reduced binding strength.

(Some figures in this article are in colour only in the electronic version)

1. Introduction

The dynamic reorganization of the CSK is essential for numerous mechanical activities of living cells, including intracellular transport, cell spreading, division and crawling. A simple approach to analyze CSK dynamics is to bind micron- or submicron-sized particles, usually spherical beads, to the

CSK of adherent cells and follow their spontaneous motion. The word ‘spontaneous’ in this context simply indicates that the bead shows movements in the absence of externally applied forces.

To establish a connection to the CSK, the beads are coated with extracellular matrix proteins such as collagen, fibronectin, or other ligands, e.g. antibodies, that bind to cell surface adhesion receptors of the integrin family [1]. Tightly bound beads can move over appreciable distances only if the CSK structure to which they are connected rearranges [2–4].

¹ Address for correspondence: Center for Medical Physics and Technology, Department of Physics, University of Erlangen-Nuremberg, Henkestrasse 91, 91052 Erlangen, Germany.

Specifically, the spontaneous bead motion is determined by force fluctuations within the CSK network that originate from myosin motor activity and the formation and depolymerization of CSK filaments. A physical description of this spontaneous, non-Brownian, superdiffusive bead motion and the underlying non-thermal driving forces can be found in [5–8].

It is less clear, however, to what degree the spontaneous bead motion is also determined by the dynamics of the connection between the bead and the cell, and whether the bead motion is sensitive to bead size and coating. Published data are inconclusive. Beads bound to the cell membrane but not to the CSK have been reported to be highly diffusive, whereas beads bound to the CSK were much less diffusive on short timescales but exhibited superdiffusive motion at longer timescales [7].

According to data published so far [7, 9], it apparently made no difference whether the beads were connected to the CSK specifically through integrin-mediated focal adhesions (such as for beads coated with an RGD-containing peptide or with fibronectin), or if the connection was less specific (such as for beads coated with poly-L-lysine or with concanavalin A).

In the case of beads coated with integrin ligands, however, numerous signal transduction pathways are activated that lead to the recruitment of focal adhesion proteins and the restructuring of the actin CSK around the bead [10–12]. Focal adhesion formation, actin reinforcement, and spontaneous bead motion have been shown to depend on the specific integrins engaged, the ligand density, the bead size, the location of the bead in relation to the cell, the presence of external forces acting on the bead, and the duration of bead binding [9, 12–14]. It would be surprising if none of these details have any effect on the observed bead motion.

In the present study, we systematically alter bead size, bead coating and bead binding time. Bead motion is analyzed in terms of mean square displacement (MSD), persistence, and bead–nucleus distance. We find that bead motion after long binding times is hardly affected by bead size, coating details, and position. The binding time after which the beads approached this nearly steady state behavior, however, is highly dependent on bead size and coating. These data indicate that after firm adhesion of the beads to the cell–matrix adhesion receptors, the bead motion only reports but does not drastically influence the ongoing reorganization of the CSK. This interpretation of the data is illustrated with a simple model consisting of a bead embedded in a viscous fluid, whereby the bead dynamically binds via an elastic spring to a pre-existing, continuously moving cytoskeletal network.

2. Materials and methods

2.1. Cell culture

MeWo skin carcinoma cells were maintained on plastic culture dishes (Nunc Surface) in Dulbecco's modified Eagle's medium (DMEM with 1 g l⁻¹ glucose) supplemented with 10% fetal calf serum, 2 mM L-glutamine, and 100 U ml⁻¹ penicillin–streptomycin (P/S) at 37 °C in humidified air containing 5% CO₂. 24–48 h prior to measurements, adherent cells were harvested with Accutase (PAA Laboratories,

Austria). 4 × 10⁵ cells were plated in ∅ 35 mm culture dishes (Nunc Surface) and incubated in 2 ml DMEM at 5% CO₂ and 37 °C.

2.2. Integrin expression

Expression levels of different integrin receptors at the surface of MeWo cells were measured using a fluorescence-activated cell sorter (FACScalibur, Becton Dickinson) as described in [15].

2.3. Beads

0.5, 1 and 2 μm carboxylated beads (Molecular Probes, Eugene, USA) and 4.5 μm epoxytated polystyrene beads (Dynal M-450 Epoxy) were coated with human fibronectin (100 μg (Roche Diagnostics) in 1 ml PBS per 1 mg of beads) or poly-L-lysine (1 ml of 0.01% (w/v) solution (Sigma) per 1 mg of beads). Binding of FN-coated beads to cells was specific to β1 integrins and could be nearly completely blocked by addition of a neutralizing β1 integrin subunit antibody (Beckton Dickinson clone 9EG7) prior to bead addition. Moreover, 4.5 μm epoxytated polystyrene beads (Dynal M-450 Epoxy) were coated with bovine serum albumin (BSA, 100 μg in 1 ml PBS per 1 mg beads) or with antibodies (mouse anti-human, 50 μg in 1 ml PBS per 1 mg beads) against specific integrins (αvβ3 (Chemicon, #MAB1976Z), αvβ5 (Chemicon, #MAB1961Z) or integrin subunits (α3 (GeneTex, #GTX75609), α5 (SouthernBiotech, #9645-01), β1 SouthernBiotech, #9375-01)).

Approximately 2 × 10⁵ beads were added to individual wells and incubated for a defined duration prior to measurements. Unbound beads were removed by washing the cells with medium. For measurements at short times (2–10 min) after bead addition, cells were not washed. To avoid measurement bias, beads that are not bound to cell–matrix adhesion receptors but instead have settled on the plastic surface of the cell culture dish were not considered. These beads can be easily recognized by their subdiffusive and strongly antipersistent behavior. During measurements, the wells were placed in an incubation chamber (humidified air with 5% CO₂ at 37 °C) mounted on the microscope.

2.4. Spontaneous bead movements

Phase contrast or fluorescent images were recorded every 120 ms with a charge-coupled device camera (Hamamatsu Orca-ER) mounted on an inverted microscope (Leica DMI-6000B) equipped with a 10×, 0.3 NA objective. The microscope was placed on a vibration isolation table (Newport). Bead positions of typically 50–200 beads per field of view were tracked continuously for 5–40 min (accuracy 10 nm (rms)) [16]. Bead positions were corrected for microscope stage drift [2], and the mean square displacement (MSD) was computed for each bead as

$$\langle \Delta r^2(\Delta t) \rangle = \langle (\mathbf{r}(t + \Delta t) - \mathbf{r}(t))^2 \rangle_t \quad (1)$$

where \mathbf{r} is the position of the bead, Δt is the time lag, and the brackets indicate time averages. A three-parameter equation

$$\langle \Delta r_{\text{fit}}^2(\Delta t) \rangle = c + D(\Delta t/t_0)^\beta \quad (2)$$

was fitted to the MSD data of each bead by minimizing the squared differences between the logarithm of the data and the logarithm of the fit equation, summed over all Δt [5]. t_0 was set arbitrarily to 1 s.

2.5. Turning angle

Directional changes in bead motion were characterized by the turning angles, $\Delta\phi(t, \Delta t)$, of two successive trajectory segments of duration Δt [5]. From the turning angle distribution, an index of directionality, or persistence of motion, p_ϕ , was calculated as the difference between the probability of forward motion ($-\pi/2 < \Delta\phi < \pi/2$) and backward motion:

$$p_\phi = 2 \left(\int_{-\pi/2}^{\pi/2} d\Delta\phi f_{\Delta\phi} \right) - 1 \quad (3)$$

where f is the probability density and the integral is taken over all turning angles $\Delta\phi$. The index of directionality p_ϕ can take values between -1 and $+1$. A value of $p_\phi < 0$ indicates antipersistent (anticorrelated) motion and is usually seen in beads with subdiffusive behavior ($\beta < 1$); $p_\phi = 0$ indicates directionally random motion associated with Brownian diffusive behavior ($\beta = 1$); $p_\phi > 0$ indicates directed (persistent, correlated) motion that is associated with superdiffusive behavior ($\beta > 1$) [5].

2.6. Estimation of bead–nucleus distance

Cell nuclei were stained with $1 \mu\text{g ml}^{-1}$ Hoechst 33342 dye. Bead–nucleus distance was defined as the Euclidean distance in the x – y -plane between the bead center and the nearest border of the nucleus. Beads located within the outline of the nucleus were assigned a distance of zero.

2.7. Model

To account for the experimental data, we propose a simple model consisting of a bead that is embedded in a viscous fluid with non-thermal Brownian force fluctuations. The bead connects to a pre-existing CSK network via an elastic spring. Based on experimental and theoretical studies published previously [5, 6], we assume that the dynamically reorganizing CSK performs a superdiffusive random motion that is not affected by the bead. The coupling between the bead and the CSK is characterized by the stiffness of the spring and the viscosity of the surrounding fluid. In the limiting case of an unbound bead with zero spring stiffness, the bead will only show Brownian fluctuations. As the link becomes stronger, the bead fluctuations will be subjected to both, the forces from the fluid and from the CSK. For the limiting case of a rigid bead–CSK-link, the bead will precisely follow the superdiffusive motion of the CSK. Thus, the model can be used to estimate the state of bead binding and internalization from the measured

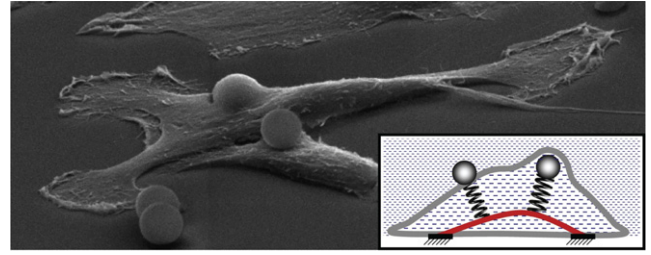


Figure 1. Scanning electron micrograph of an adherent cell with beads in different stages of internalization. The inset illustrates our model of a bead coupled to the cytoskeleton (red) by a spring with spring constant k . The viscous damping constant γ is larger for an internalized bead.

MSD. It does not attempt to explain bead binding dynamics or the superdiffusive motion of the CSK, however.

The CSK consists of contractile filaments that are interconnected by various types of cross-linkers and are anchored to the extracellular matrix at distinct focal adhesion points. Biophysical remodeling activity, such as attachment and detachment of myosin cross-linkers or (de-)polymerization of actin, leads to ongoing spatial fluctuations of this network and occasionally to major topological reorganizations. Let p be an arbitrary point on the network (e.g., some marked local feature on a filament or a specific node). We model the motion $\mathbf{r}_p(t)$ of point p by a stationary superdiffusive random walk in two dimensions, $\mathbf{r}_p(t) = (x_p(t), y_p(t))$ with an MSD that is characterized by an apparent diffusivity D and a fractional power-law exponent β . The numerical method to generate such anomalous random walks is described in appendix.

The bead (at position $\mathbf{r}(t)$) is described as an overdamped particle, subject to linear friction forces $-\gamma d/dt \mathbf{r}(t)$ and white-noise, Gaussian force fluctuations $\Delta\mathbf{F}(t)$ from the surrounding viscous medium. Since the cell membrane and cell cortex are in a non-equilibrium state, an Einstein relation between damping and fluctuations is not valid here [8]. Moreover, a part of the apparent velocity fluctuations observed for unbound beads at the membrane may be due to uncorrelated measurement noise. Experimental data show that the amplitude of the unbound bead fluctuations is typically larger than expected from thermal origins.

The bead is coupled to a single anchor point $p = a$ of the CSK network by an elastic spring with zero rest length and stiffness k (figure 1). When displaced from the anchor point \mathbf{r}_a , the bead experiences a drag force $k(\mathbf{r}_a(t) - \mathbf{r}(t))$. We treat the trajectory of the anchor point $\mathbf{r}_a(t)$ as a pre-defined random process that is not affected by the motion of the attached bead. At any time t , the total force on the bead is given by

$$\mathbf{F}(t) = -\gamma d/dt \mathbf{r}(t) + \Delta\mathbf{F}(t) + k(\mathbf{r}_a(t) - \mathbf{r}(t)). \quad (4)$$

In our overdamped approximation, we set $\mathbf{F}(t) = \mathbf{0}$ and obtain a stochastic differential equation for the bead trajectory $\mathbf{r}(t)$,

$$d/dt \mathbf{r}(t) = [k(\mathbf{r}_a(t) - \mathbf{r}(t)) + \Delta\mathbf{F}(t)]/\gamma, \quad (5)$$

which is solved numerically.

3. Results and discussion

3.1. Modeling of bead fluctuations

From the numerical solutions of the stochastic differential equation (equation (5)) in various parameter regimes, we obtain bead trajectories from which we compute the mean squared displacement (MSD) as a function of lag time Δt (figure 2). For an unbound bead, one obtains a purely diffusive motion, characterized by a MSD increasing linearly with time. If the bead is bound to a non-moving anchor point via a linear elastic spring, the amplitude of the random motion is restricted, leading to an asymptotic plateau in the MSD (figure 2(a)). The characteristic lagtime τ_{rel} which separates the diffusive regime from the plateau regime is the inverse of the visco-elastic relaxation rate

$$R = k/\gamma. \quad (6)$$

The choice of the model parameter β is based on measurements that show that CSK fluctuates with a MSD that grows according to a pure superdiffusive power-law with typically $\beta = 1.5$ [2, 5, 8, 15]. Curves (b)–(d) correspond to cases of decreasing binding strength of the bead to the CSK. In the case of intermediate binding strength (curves (b) and (c)), the MSD is diffusive for small Δt and becomes superdiffusive for larger Δt . Interestingly, in the transition regime one finds a subdiffusive behavior (effective $\beta < 1$). In the more strongly bound case (b), the MSD exhibits a plateau at small Δt and a crossover to a superdiffusive behavior at longer timescales. For the extreme case of rigid binding (a), the bead reports exclusively the fluctuations of the CSK, and the MSD is purely superdiffusive. Note that in the above simulation, we have chosen a smaller D for the CSK fluctuations relative to the Brownian diffusion constant of the unbound bead. This choice accounts for our experimental data that always show an inverse correlation between D and β .

3.2. Initial bead binding

Fibronectin-coated beads were bound to cells for 2 min, immediately followed by a continuous 20 min recording of the bead trajectory during spontaneous motion. The trajectories were subdivided into 1 min sections. For each section, the mean square displacement (MSD), the velocity (averaged over 3 s), and the persistence were computed.

For these very short bead binding times, only 19% of the beads showed pronounced superdiffusive behavior with a power-law exponent β of the MSD larger than 1.3. The remaining beads moved diffusively or subdiffusively. Over 20 min, most of these beads showed a transition to pronounced superdiffusive behavior ($\beta > 1.3$). An example for such a transition is shown in figure 3. This transition was characterized by a sudden increase, both of the power-law exponent β of the MSD, and the degree of persistence. At the same time, the apparent diffusivity D and the velocity decreased. According to our model, such behavior indicates the transition from an essentially unbound to a strongly bound state of the bead.

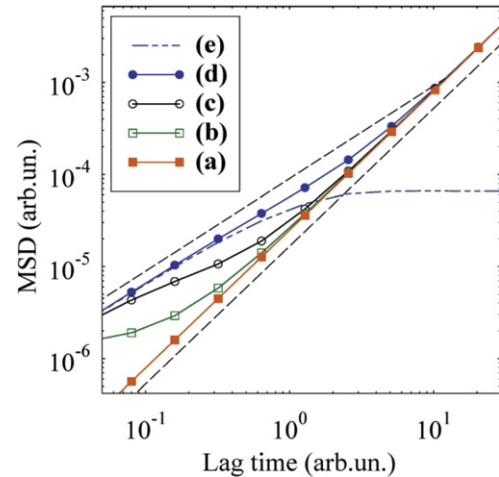


Figure 2. Mean squared displacement computed for an overdamped particle that undergoes Brownian fluctuations and is coupled by a spring to the CSK with long time correlated spatial fluctuations. Upper dashed line: diffusive power-law (exponent 1). Lower dashed line: fractional power-law with exponent 1.5. Lines (a)–(d): particle MSDs for increasing relaxation times ($\tau_{\text{rel}} = 1/R = 0.001, 0.01, 0.1, 1$). Line (e): MSD of a particle coupled to a fixed anchor point.

For further analysis, the bead trajectories were divided into the pre-transition and the post-transition phase. For each phase, the MSD was then calculated separately. The average apparent diffusivity D decreased five-fold from pre-transition to post-transition phase, whereas the average power-law exponent β increased from 0.79 to 1.50 (figures 3(E) and (F)).

The pre-transition phase corresponds to initial adhesion to integrins. Such adhesions have been shown to form typically within 60–90 s after presenting fibronectin-coated beads to the cell surface [12, 17, 18]. The bead trajectory at this phase is characterized by large, slightly subdiffusive movements ($\beta = 0.79$, large D), suggesting that the initially formed fibronectin–integrin bonds are not yet tightly connected to the CSK. After some time, the step size of the movements becomes abruptly smaller, as seen in the sudden decrease of D (figure 3(C)), while the bead trajectory becomes more directed and superdiffusive ($\beta = 1.50$, figure 3(D)) suggesting that the fibronectin–integrin bonds are now tightly connected to the underlying CSK, presumably through integrin clustering and focal adhesion formation [10, 19, 20].

The transition from a weakly bound to a tightly bound state occurred within a time frame of typically 1–2 min. This bi-phasic ‘all-or-nothing’ response of the bead movement indicates that the dynamics of the adhesion formation process is important only insofar as it sets the time point when a tight bead–CSK connection has been established. Averaging D and β over the first 20 min (figures 3(G) and (H)) masked the ‘all-or-nothing’ response of the individual beads because the transition from a poorly to a tightly bound state occurred at different time points, as observed by the continuing changes in the percentage of tightly bound beads versus time (figure 3(H)). The percentage of tightly bound beads was highly correlated with the average power-law exponent β (figure 3(H)).

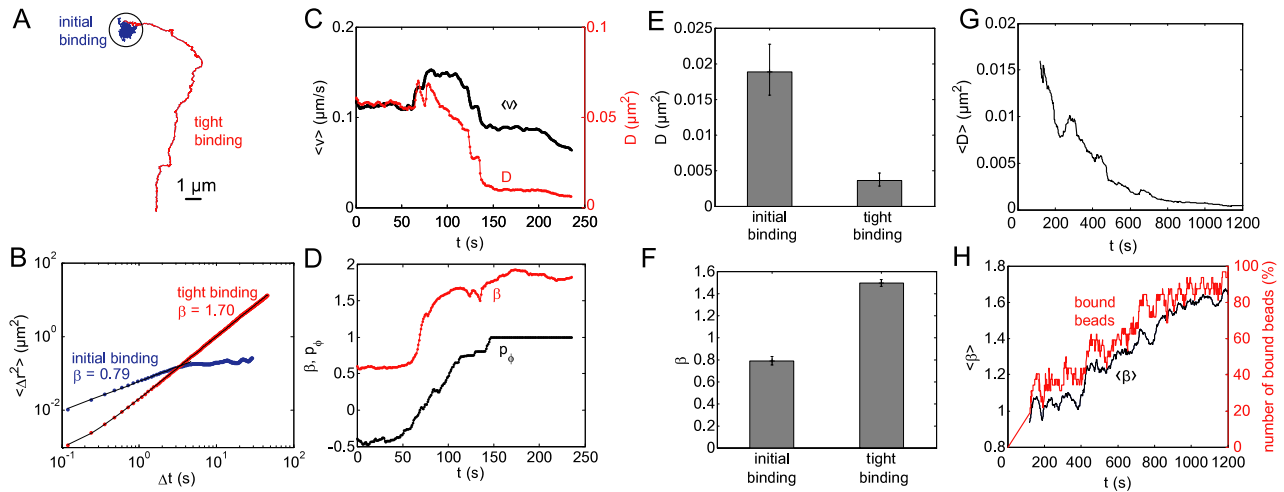


Figure 3. (A)–(D) Binding process of a 4.5 μm fibronectin-coated bead. (A) The trajectory shows a transition from an initial bead binding phase (circle) to a tight bead binding phase. (B) MSD of the same trajectory calculated separately for both phases. (C) and (D) The transition from loose to tight binding was accompanied by a sudden increase in the power-law exponent β and persistence p_ϕ , as well as a decrease in the velocity v and the apparent diffusivity D . During the transition, both v and D commonly exhibit a brief transient increase. (E) and (F) Average power-law exponent β (mean \pm stdev) and apparent diffusivity D (geometric mean \pm stdev) computed separately for the initial and tight binding phase. Only beads that displayed a clear transition between the two phases were considered for this evaluation ($n = 34$). (G) and (H) Average apparent diffusivity D (geometric mean), power-law exponent β , and percentage of bound beads (defined as $\beta > 1.3$) versus bead binding time.

3.3. Bead coating

The dynamics of adhesion formation has been reported to depend on ligand type and density, and number of available ligands per adhesion site [12, 21, 22]. We tested the effect of different ligands and number of ligands per adhesion site by studying the motion of beads with different coatings and sizes.

Beads were coated with fibronectin, with antibodies against specific integrins ($\alpha v\beta 3$, $\alpha v\beta 5$) or integrin subunits ($\beta 1$, $\alpha 3$, $\alpha 5$), with poly-L-lysine (PLL), or with bovine serum albumin (BSA). Fibronectin binds to several integrin receptors including $\alpha 5\beta 1$, $\alpha v\beta 1$, $\alpha v\beta 3$ and $\alpha 4\beta 1$ [23–25]. PLL binds non-specifically via electrostatic interactions to the cell surface and establishes connections with cortical actin structures without the formation of focal adhesion complexes [26]. Beads coated with BSA are assumed to adsorb non-specifically to the cell surface and do not form connections with the CSK [1, 7].

BSA-coated beads displayed nearly diffusive behavior (β close to unity) and an apparent diffusivity D that was more than ten-fold higher compared to other coatings (figures 4(A) and (B)). This confirms that BSA-coated beads are not properly connected to the CSK and do not report ongoing CSK remodeling processes [1, 7].

Only small differences were observed in the spontaneous motion of beads coated with fibronectin, integrin antibodies, or PLL when measured 30 min after bead addition (figures 4(A) and (B)). The power-law exponent β showed pronounced superdiffusivity, which indicates tight bead attachment to the CSK. Larger exponents β were associated with lower apparent diffusivity D . The small differences in β and D seen in the beads coated with integrin antibodies (figures 4(A) and (B)) did not correlate with integrin receptor expression levels and cannot be explained by the activation of subunit-specific

integrin signaling pathways, since PLL-coated beads that do not activate integrins moved similarly.

3.4. Bead size

The motion of 1 and 4.5 μm PLL-coated beads after 30 min of binding was similar, with a slightly more pronounced superdiffusivity (smaller D , larger β) for the 1 μm beads (figures 4(C) and (D)). In contrast, the motion of fibronectin-coated beads after 30 min of binding showed clear size-dependence with more pronounced superdiffusivity for larger beads. Previous studies have shown that substantially more focal adhesion proteins are recruited around larger fibronectin-coated beads compared to smaller beads [12]. Since no such recruitment occurs in the case of PLL-coated beads, this may explain the different sensitivity to bead size. Further experiments revealed that the size-dependent dynamics of fibronectin-coated beads originate from differences in the binding dynamics, not binding strength: for example, if fibronectin-coated beads are measured after a binding time of 20 min, the size-dependence is reversed: now the smaller beads appear more superdiffusive (figures 4(C) and (D)). These population averaged data are consistent with the assumption that only the fraction of beads that are tightly bound to the CSK changes over time, depending on bead size. The strength of the binding, or the statistics of the underlying CSK movements, however, remain unchanged. In this context, although the bead motion on confluent, stationary cells is less centripetally directed than on highly dynamic lamellipodia, the mechanism driving the bead motion appears identical in both cases: the beads are set in motion when they couple to the cortical actin flow that is largely unaffected by bead size and coating details [27, 28].

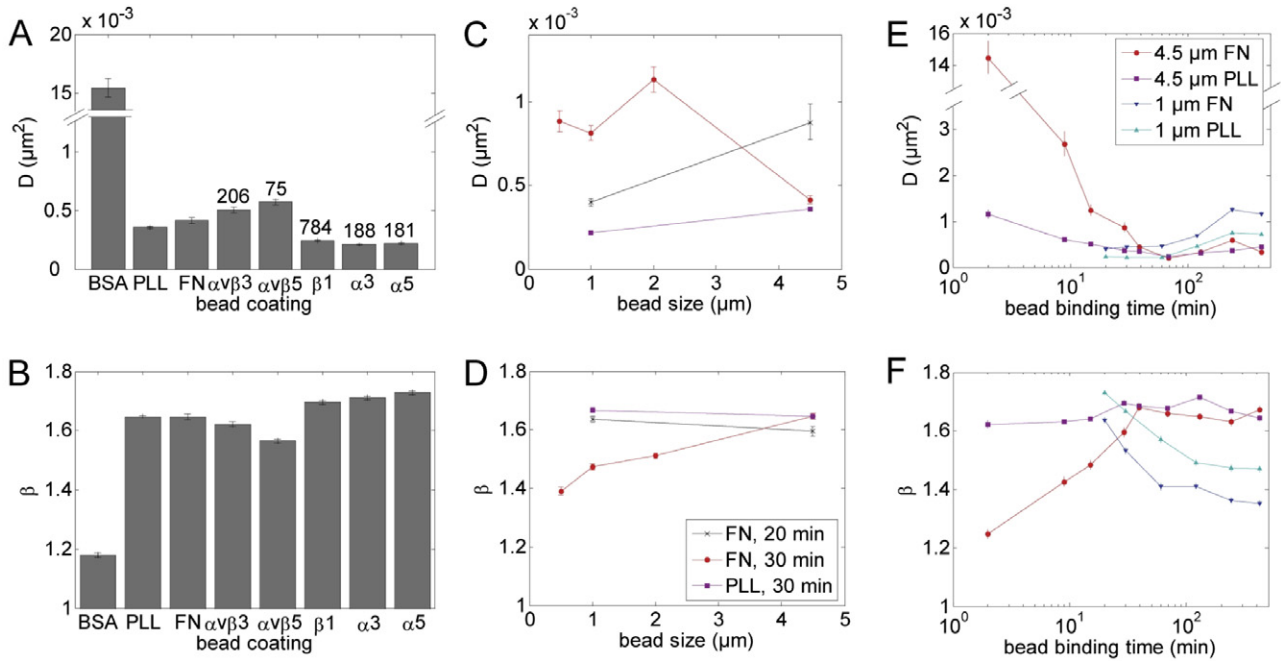


Figure 4. Fit parameters of the MSD averaged over individual beads bound to MeWo cells for different bead coatings, sizes, and binding times. (A) Geometric mean of apparent diffusivity D (\pm stderr). Bead diameter: $4.5 \mu\text{m}$, binding time: 30 min. Numbers above bars indicate the expression levels of integrins relative to isotype controls (delta mean fluorescence). (B) Mean of the power-law exponent β (\pm stderr). (C) and (E) Geometric mean of apparent diffusivity D (\pm stderr); (D) and (F) mean of the power-law exponent β (\pm stderr).

3.5. Long bead binding times

Fibronectin- or PLL-coated beads with a diameter of $4.5 \mu\text{m}$ or $1 \mu\text{m}$ were incubated with the cells for 2–420 min. The MSD was calculated for individual beads, and the average of the individual fit parameters was taken over all beads. The apparent diffusivity D and the exponent β of the MSD showed a bi-phasic time-dependence (figures 4(E) and (F)). D was high at the beginning of the binding process for $4.5 \mu\text{m}$ fibronectin-coated beads because only a small fraction of the beads was tightly bound to the CSK. Within 30 min, however, D decreased dramatically and β increased from 1.25 to 1.66. In contrast to $4.5 \mu\text{m}$ fibronectin-coated beads, $4.5 \mu\text{m}$ PLL-coated beads appeared to be already bound to the CSK after 2 min, and the subsequent decrease in D and increase in β over the next 30 min was small. After 30 min, D and β for both PLL- and fibronectin-coated beads saturated at a highly superdiffusive value, indicating that the bead–CSK link remained stable over several hours.

Beads of $1 \mu\text{m}$ diameter behaved differently. Due to the low speed of bead settlement onto the cell surface, measurements could not be started immediately after bead addition. Therefore, the expected initial increase in superdiffusive behavior could not be observed. Yet, the data starting 20 min after bead addition indicate a shift from a highly superdiffusive towards a less superdiffusive behavior over the following 30 min (figures 4(E) and (F)). The decrease in the superdiffusive behavior can be explained by the internalization of the beads. A bead that has been internalized experiences a higher viscosity (proportional to γ) in the crowded cytoplasm, compared to a non-internalized bead. At the same time, the tight connections to the CSK may become

weaker, leading to a smaller k , as integrin receptors and focal adhesion proteins become internalized and are subsequently degraded. According to equation (6), both effects lead to smaller relaxation rates. For individual internalized beads in a state of weak binding, our model predicts a characteristic MSD with three distinct lagtime regimes. Indeed, such behavior was frequently observed for $1 \mu\text{m}$ fibronectin- as well as PLL-coated beads measured at long bead binding times. A typical example of a $1 \mu\text{m}$ fibronectin-coated bead measured after a binding time of 420 min is shown in figure 5. Near diffusive motion is observed at short timescales ($\Delta t < 1 \text{ s}$, $\beta = 1.24$), subdiffusive motion at intermediate timescales ($\beta = 0.73$), and superdiffusive motion at longer timescales ($\Delta t > 20 \text{ s}$, $\beta = 1.49$) (figures 5(A) and (B)). These three phases are also evident in the degree of persistence p computed from the turning angle of bead motion. At short timescales, bead motion is random, becomes antipersistent at intermediate timescales and persistent at longer timescales (figure 5(C)).

3.6. Bead–nucleus distance

Persistent, superdiffusive and sometimes ballistic motion of beads coated with integrin ligands towards the cell’s nucleus has previously been reported in several studies in which beads were placed with an optical trap onto a lamellipodium [3, 9, 11, 13]. This persistent bead motion and has been interpreted as the signature of the retrograde actin flow within the lamellipodium. Bead motion in these studies was followed for several seconds up to several minutes; as the beads approached the cell’s central region, the persistent motion stalled and became more random [9].

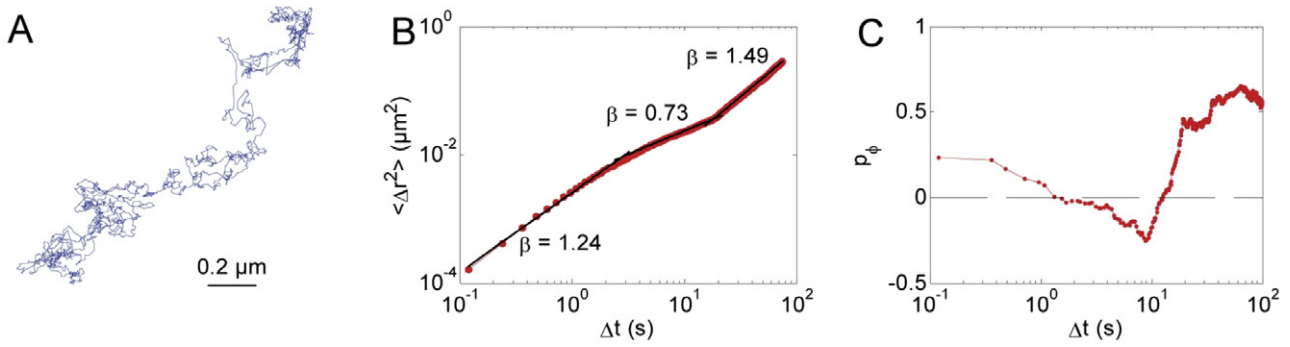


Figure 5. (A) Typical bead trajectory of a 1 μm diameter, fibronectin-coated bead measured for a bead binding time of 420 min. (B) The mean square displacement shows diffusive, caged, and superdiffusive regimes. (C) The transition between these three regimes can also be distinguished by the degree of persistence as a function of time lag.

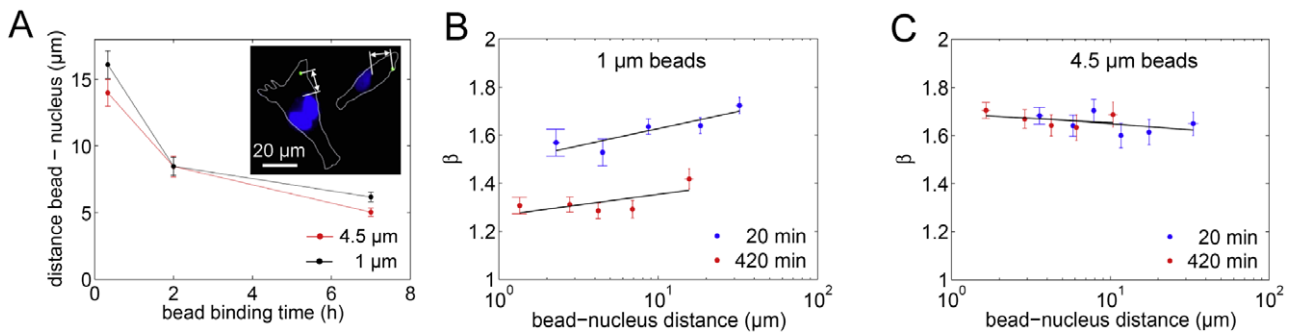


Figure 6. Dependence of bead motion on bead–nucleus distance. (A) Bead–nucleus distance was measured at bead binding times of 20, 120 and 420 min as the Euclidean distance between the bead center and the nearest border of the nucleus (inset). Both 1 and 4.5 μm FN-coated beads tend to move towards the cell nucleus. (B) and (C) The power-law exponent β is weakly but significantly ($p < 0.05$) dependent on the bead–nucleus distance for 1 μm beads (B) but not for 4.5 μm beads (C).

In this study, we observed bead motion from 20 min up to several hours of bead binding, yet even at these long time intervals, we could detect a tendency of fibronectin-coated beads to move towards the cell’s nucleus (figure 6(A)). Interestingly, the beads were still superdiffusive even close to the nucleus, although the power-law exponent β for 1 μm beads but not for 4.5 μm beads depended weakly on the distance to the nucleus (figures 6(B) and (C)). These data indicate that bead motion for long binding times is not dominated by rearward actin flow but is mostly driven by ongoing force fluctuations due to dynamic reorganization processes within the pre-stressed actin network [5].

4. Conclusions

We have established that nanoscale particle tracking can probe the reorganization dynamics of the CSK structures, provided that the particle is tightly bound to these structures. In particular, our data support the notion of beads as passive markers. Their fluctuation statistics appears indistinguishable from those of intrinsic CSK markers that are tracked by speckle microscopy or similar techniques [29]. However, the process of bead attachment to the CSK is highly dynamic and depends on bead size and coating. Therefore, the bead binding time should be carefully chosen such that the beads are given the opportunity to bind tightly to the CSK, but not

so long that the linkage to the CSK degrades after the beads are internalized. Our findings may also be important for the design and interpretation of micro-rheology studies in which cell mechanical properties are measured using ligand-coated beads that are optically or magnetically forced [1, 8, 16].

Acknowledgments

We thank Wolfgang H Goldmann for helpful discussions, and Barbara Reischl and Christine Albert for technical assistance. This work was supported by grants from the Deutsche Forschungsgemeinschaft (FA336/2-1), Deutsche Krebshilfe (107384) and the National Institutes of Health (HL65960).

Appendix. Generation of superdiffusive fluctuations

In the following we describe a method to generate particle trajectories $x(t)$ with a prescribed MSD in the form of a power-law with fractional exponent β . For stationary fluctuations, the MSD can be expressed by the velocity autocorrelation function,

$$\langle x^2 \rangle(t) = \int_0^t 2(t - \tau) C_{vv}(\tau) d\tau,$$

the Fourier transform of which is the spectral power density,

$$F\{C_{vv}(\tau)\} = P(\omega) = |v(\omega)|^2.$$

To guarantee that $\langle x^2 \rangle(t) \sim t^\beta$, it is sufficient to ensure that the amplitudes of the velocity components fall with frequency as $|v(\omega)| \sim \omega^{(1-\beta)}$. The phases of the velocity components can be chosen arbitrarily, as far as only the MSD is concerned. We have discretized the frequencies ω_k and assigned to $v(\omega_k)$ complex values with magnitude $|\omega^{(1-\beta)}|$ and random phases that are distributed equally between 0 and 2π . Using a discrete fast Fourier transform, we obtain from $v(\omega_k)$ the velocity fluctuations $v(t_n)$ in the time domain. Finally, the trajectory $x(t_n)$ is obtained by integration over $v(t_n)$. The y-components of the particle were generated independently, giving a 2D trajectory of the desired properties.

References

- [1] Wang N, Butler J P and Ingber D E 1993 Mechanotransduction across the cell surface and through the cytoskeleton *Science* **260** 1124–7
- [2] An S S, Fabry B, Mellema M, Bursac P, Gerthoffer W T, Kayyali U S, Gaestel M, Shore S S and Fredberg J J 2004 Role of heat shock protein 27 in cytoskeletal remodeling of the airway smooth muscle cell *J. Appl. Physiol.* **96** 1701–13
- [3] Caspi A, Granek R and Elbaum M 2000 Enhanced diffusion in active intracellular transport *Phys. Rev. Lett.* **85** 5655–8
- [4] Sheetz M P, Felsenfeld D P and Galbraith C G 1998 Cell migration: regulation of force on extracellular-matrix-integrin complexes *Trends Cell Biol.* **8** 51–4
- [5] Raupach C, Zitterbart D P, Mierke C T, Metzner C, Muller F A and Fabry B 2007 Stress fluctuations and motion of cytoskeletal-bound markers *Phys. Rev. E* **76** 011918
- [6] Metzner C, Raupach C, Paranhos Zitterbart D and Fabry B 2007 Simple model of cytoskeletal fluctuations *Phys. Rev. E* **76** 021925
- [7] Bursac P, Fabry B, Treppe X, Lenormand G, Butler J P, Wang N, Fredberg J J and An S S 2007 Cytoskeleton dynamics: fluctuations within the network *Biochem. Biophys. Res. Commun.* **355** 324–30
- [8] Bursac P, Lenormand G, Fabry B, Oliver M, Weitz D A, Viasnoff V, Butler J P and Fredberg J J 2005 Cytoskeletal remodelling and slow dynamics in the living cell *Nat. Mater.* **4** 557–61
- [9] Caspi A, Yeger O, Grosheva I, Bershadsky A D and Elbaum M 2001 A new dimension in retrograde flow: centripetal movement of engulfed particles *Biophys. J.* **81** 1990–2000
- [10] Plopper G and Ingber D E 1993 Rapid induction and isolation of focal adhesion complexes *Biochem. Biophys. Res. Commun.* **193** 571–8
- [11] Choquet D, Felsenfeld D P and Sheetz M P 1997 Extracellular matrix rigidity causes strengthening of integrin-cytoskeleton linkages *Cell* **88** 39–48
- [12] Galbraith C G, Yamada K M and Sheetz M P 2002 The relationship between force and focal complex development *J. Cell Biol.* **159** 695–705
- [13] Schmidt C E, Horwitz A F, Lauffenburger D A and Sheetz M P 1993 Integrin–cytoskeletal interactions in migrating fibroblasts are dynamic, asymmetric, and regulated *J. Cell Biol.* **123** 977–91
- [14] Deng L, Fairbank N J, Fabry B, Smith P G and Maksym G N 2004 Localized mechanical stress induces time-dependent actin cytoskeletal remodeling and stiffening in cultured airway smooth muscle cells *Am. J. Physiol. Cell Physiol.* **287** C440–8
- [15] Mierke C T, Zitterbart D P, Kollmannsberger P, Raupach C, Schlotzer-Schrehardt U, Goecke T W, Behrens J and Fabry B 2008 Breakdown of the endothelial barrier function in tumor cell transmigration *Biophys. J.* **94** 2832–46
- [16] Fabry B, Maksym G N, Shore S A, Moore P E, Panettieri R A Jr, Butler J P and Fredberg J J 2001 Time course and heterogeneity of contractile responses in cultured human airway smooth muscle cells *J. Appl. Physiol.* **91** 986–94
- [17] DePasquale J A and Izzard C S 1987 Evidence for an actin-containing cytoplasmic precursor of the focal contact and the timing of incorporation of vinculin at the focal contact *J. Cell Biol.* **105** 2803–9
- [18] Izzard C S 1988 A precursor of the focal contact in cultured fibroblasts *Cell Motil. Cytoskeleton* **10** 137–42
- [19] Gallant N D, Michael K E and Garcia A J 2005 Cell adhesion strengthening: contributions of adhesive area, integrin binding, and focal adhesion assembly *Mol. Biol. Cell* **16** 4329–40
- [20] Hu K, Ji L, Applegate K T, Danuser G and Waterman-Storer C M 2007 Differential transmission of actin motion within focal adhesions *Science* **315** 111–5
- [21] Chen C S, Alonso J L, Ostuni E, Whitesides G M and Ingber D E 2003 Cell shape provides global control of focal adhesion assembly *Biochem. Biophys. Res. Commun.* **307** 355–61
- [22] Reinhart-King C A, Dembo M and Hammer D A 2005 The dynamics and mechanics of endothelial cell spreading *Biophys. J.* **89** 676–89
- [23] Fogerty F J, Akiyama S K, Yamada K M and Mosher D F 1990 Inhibition of binding of fibronectin to matrix assembly sites by anti-integrin (alpha 5 beta 1) antibodies *J. Cell Biol.* **111** 699–708
- [24] Yang J T and Hynes R O 1996 Fibronectin receptor functions in embryonic cells deficient in $\alpha_5\beta_1$ integrin can be replaced by α_V integrins *Mol. Biol. Cell* **7** 1737–48
- [25] Sechler J L, Cumiskey A M, Gazzola D M and Schwarzbauer J E 2000 A novel RGD-independent fibronectin assembly pathway initiated by alpha4beta1 integrin binding to the alternatively spliced V region *J. Cell Sci.* **113** 1491–8
- [26] Rivelino D, Zamir E, Balaban N Q, Schwarz U S, Ishizaki T, Narumiya S, Kam Z, Geiger B and Bershadsky A D 2001 Focal contacts as mechanosensors: externally applied local mechanical force induces growth of focal contacts by an mDia1-dependent and ROCK-independent mechanism *J. Cell Biol.* **153** 1175–86
- [27] Abercrombie M, Heaysman J E and Pegrum S M 1970 The locomotion of fibroblasts in culture. 3. Movements of particles on the dorsal surface of the leading lamella *Exp. Cell Res.* **62** 389–98
- [28] Dembo M and Harris A K 1981 Motion of particles adhering to the leading lamella of crawling cells *J. Cell Biol.* **91** 528–36
- [29] Waterman-Storer C M, Desai A, Bulinski J C and Salmon E D 1998 Fluorescent speckle microscopy, a method to visualize the dynamics of protein assemblies in living cells *Curr. Biol.* **8** 1227–30